Наносистеми, наноматеріали, нанотехнології
Nanosistemi, Nanomateriali, Nanotehnologii
2026, т. 24, № 1, сс. 175–187
https://doi.org/10.15407/nnn.24.01.0175

PACS numbers: 61.72.Mm, 61.72.uj, 68.35.Ct, 68.37.Hk, 68.37.Ps, 68.55.J-, 81.15.Cd

Influence of Mn^2 and Tb^3 Activators on the Surface Morphology of GaN Thin Films

O. M. Bordun[1], I. I. Medvid[1], I. Yo. Kukharskyy[1], I. O. Bordun[1], I. M. Kofliuk[1], O. Y. Mylyo[1], V. O. Maksymiv[1], D. S. Leonov[2], and M. V. Protsak[1]

[1]*Ivan Franko National University of Lviv,*
50, Drahomanov Str.,
UA-79005 Lviv, Ukraine
[2]*Technical Centre, N.A.S. of Ukraine,*
13, Pokrovska Str.,
UA-04070 Kyiv, Ukraine

The study investigates the influence of transition (Mn) and rare-earth (Tb) dopants on the surface morphology of as-deposited GaN thin films. GaN, GaN:Mn, and GaN:Tb thin films are obtained by radio frequency (RF) ion-plasma sputtering in a nitrogen atmosphere on single-crystal Si substrates. Surface morphology studies performed using atomic force microscopy (AFM) show that the addition of Mn promotes an increase in the average grain diameter from 85 nm to 166 nm and is accompanied by a decrease in the root-mean-square roughness from 6.4 nm to 4.8 nm. An analysis of crystallite-size distributions by diameter, area, and volume is carried out, and it is suggested that anomalous secondary grain growth occurs during the RF-sputtering process, when Mn impurity is added. The addition of Tb impurity leads to an even greater increase in grain size, which is attributed to the large ionic radius of the Tb^{3+} ion and the generation of significant mechanical stresses.

У роботі проведено дослідження впливу домішок перехідних (Mn) і рідкісноземельних (Tb) елементів на морфологію поверхні свіжонанесених тонких плівок GaN. Тонкі плівки GaN, GaN:Mn і GaN:Tb одержано методом високочастотного йонно-плазмового розпорошення в атмосфері азоту на монокристалічних підкладинках Si. Дослідження морфології поверхні тонких плівок методом атомно-силової мікроскопії показали, що додавання Mn сприяє зростанню середнього діяметра зерен з 85 до 166 нм і супроводжується пониженням середньоквадратичної шерсткости від 6,4 до 4,8 нм. Проведено аналізу розподілів кристалітів за діяметром, площею й об'ємом і запропоновано, що у процесі ВЧ-

напорошення відбувається аномальний ріст вторинних зерен за додавання домішки Mn. З додаванням домішки Tb спостерігається ще більше зростання розмірів зерен, що пов'язується з великим йонним радіюсом йона Tb^{3+} і створенням сильних механічних напружень.

Key words: thin films, GaN, doping, manganese, terbium, RF sputtering, surface morphology, atomic force microscopy.

Ключові слова: тонкі плівки, GaN, леґування, Манґан, Тербій, ВЧ-розпорошення, морфологія поверхні, атомно-силова мікроскопія.

(Received 16 February, 2026)

1. INTRODUCTION

In recent years, gallium nitride (GaN) has been extensively studied by many researchers due to its widespread use in optoelectronic devices, lasers, and photodetectors [1–7]. In particular, the luminescent properties of both pure and doped GaN are widely studied, which allows for a significant expansion of the functional capabilities of this material [8–13]. In addition, GaN is widely used in power electronics [14] and is the preferred semiconductor for power converters in automotive electronics and the power supply industry [15].

Gallium nitride is an important material in the development of efficient light-emitting diodes (LEDs) [16, 17] and micro-light-emitting diodes (μLEDs) with green and blue emission, designed for integration into display systems [18]. The application of this material is not limited to these areas, as researchers have developed and tested a light-controlled artificial synapse based on gallium nitride (GaN), capable of mimicking the learning and memory processes of the human brain for the creation of ultrafast and energy-efficient neuromorphic computing systems [19].

For the practical application of semiconductor thin films in optoelectronics and instrument engineering, their morphological characteristics are quite important, since they affect the efficiency of devices created on their basis. In general, the issue of the physical properties of thin films is complicated by the fact that their structure is often far from perfect. Obtaining the required, stable, and reproducible properties of polycrystalline films is limited due to the presence of grain boundaries. The physical properties of polycrystalline thin films depend significantly not only on the characteristics of the material, but also on the energy levels that arise due to the presence of grain boundaries. It is clear that these levels are determined by the size of the crystallites that form thin films. This has led to the investigation of the surface morphology of GaN, GaN:Mn, and GaN:Tb thin films using atomic force microscopy

(AFM) and scanning electron microscopy (SEM). The thin-film samples were obtained by RF ion-plasma sputtering, which is optimal for producing homogeneous semiconductor and dielectric films [20].

2. EXPERIMENTAL TECHNIQUE

GaN, GaN:Mn, and GaN:Tb thin films with thicknesses of 0.3–0.8 μm were obtained by RF ion-plasma sputtering on monocrystalline Si substrates. RF ion-plasma sputtering was carried out in a nitrogen atmosphere in a system using a magnetic field of external solenoids for compression and additional ionization of the plasma column. The concentration of Mn^{2+} and Tb^{3+} activators was 1 mol.%. The structure and phase composition of the obtained films were investigated by x-ray diffraction analysis (Shimadzu XDR-600). The characteristic diffraction patterns of the thin films were presented previously in our work [21].

Elemental analysis of the studied samples at several points on the surface of the thin films was performed using an OXFORD INCA Energy 350 energy-dispersive spectrometer.

The surface morphologies of GaN and GaN:Mn thin films were studied using an atomic force microscope (AFM) 'INTEGRA TS-150'. Surface images of the thin films were recorded in semi-contact mode (tapping mode) in air. A silicon cantilever of the NSG10 series with a resonance frequency of 323 kHz and a stiffness of 24 N/m was used. In addition, a scanning electron microscope (JSM-7200F, Jeol) operated at an accelerating voltage of 7 kV was also employed to investigate the surface morphology of GaN, GaN:Mn, and GaN:Tb thin films.

3. RESULTS AND DISCUSSION

AFM images of the surface morphology of as-deposited GaN and GaN:Mn thin films obtained by RF ion-plasma sputtering on Si substrates are shown in Fig. 1.

For areas of identical size (5×5 μm) on the AFM surface morphology images of the studied samples, a number of standard parameters were calculated: root-mean-square roughness, average roughness, average grain diameter, average grain area and volume, grain height with maximum number of grains, coefficient of kurtosis and surface skewness. The characteristic surface roughness parameters and grain size characteristics of as-deposited GaN and GaN:Mn thin films obtained by RF ion-plasma sputtering on Si substrates are presented in Table. As can be seen from the obtained results, Mn doping significantly affects the surface roughness and grain size of

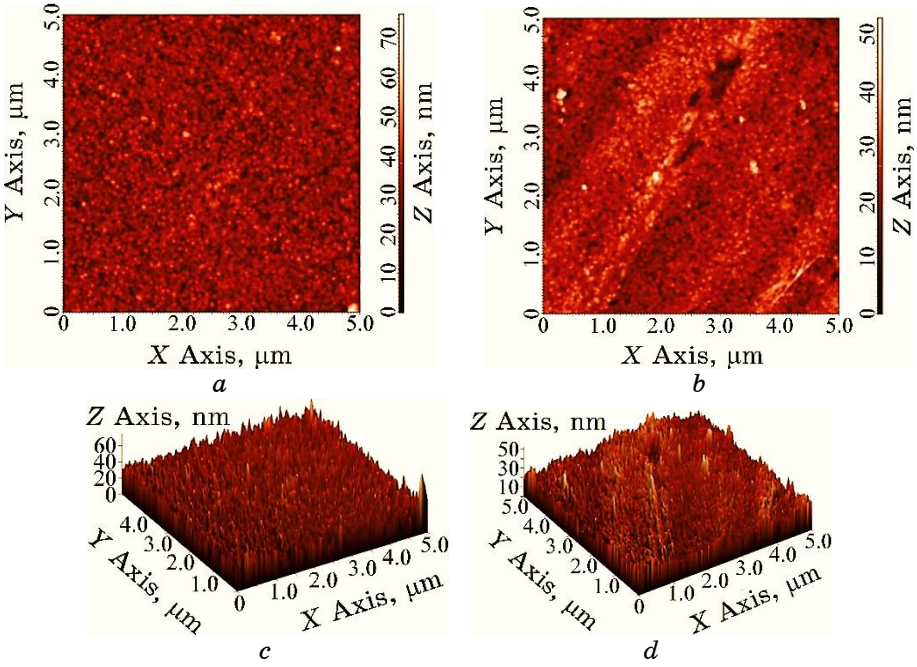

Fig. 1. AFM images of the surface morphology of as-deposited GaN (*a*, *c*) and GaN:Mn (*b*, *d*) thin films obtained by RF sputtering on Si substrates. Images *a* and *b* are two-dimensional; *c* and *d* are three-dimensional.

TABLE. Surface roughness and crystalline grain parameters of GaN and GaN:Mn thin films.

Parameter	GaN	GaN:Mn
Average grain diameter D, nm	85	166
Root mean square roughness S_q, nm	6.4	4.8
Average roughness S_a, nm	5.1	3.8
Grain height with maximum number of grains Z, nm	29	23
Average grain area S, nm^2	2660	7750
Average grain volume V, nm^3	8240	23700
Coefficient of kurtosis S_{ka}	3.7	4.0
Surface skewness S_{sk}	0.08	0.20

GaN thin films.

Analysis of the AFM images (Fig. 1), as well as the surface roughness and crystalline grain parameters (Table) of GaN and GaN:Mn thin films, shows that the grain sizes of as-deposited GaN:Mn thin films obtained by RF ion-plasma sputtering on Si sub-

strates are significantly larger compared to those of pure GaN samples. For example, the average grain diameter of GaN:Mn thin films is almost twice that of GaN films. At the same time, for GaN:Mn thin films, a decrease in both the root-mean-square and the average arithmetic surface roughness parameters by nearly 1.3 times is observed compared to the corresponding values for GaN thin films.

The increase in crystalline grain size, in particular the increase in the average grain diameter, area, and volume, along with the simultaneous decrease in parameters such as root-mean-square and average-arithmetic surface roughness, indicates a complication of the surface structure of the thin films. The S_q/S_a ratio for GaN and GaN:Mn thin films is 1.25 and 1.26, respectively, which corresponds to a normal distribution of grain heights forming the sample surface [22].

Comparison of the histograms of grain height distribution (Fig. 2) shows that Mn doping influences the formation of the surface morphology of GaN thin films obtained by RF ion-plasma sputtering on Si substrates and leads to a reduction in grain heights compared to undoped samples. The results obtained show that GaN:Mn thin films are characterized by horizontal grain growth parallel to the substrate surface.

The S_q/S_a ratio values and the grain height distribution histograms (Fig. 2) confirm that coarse structural defects are not typical for GaN and GaN:Mn thin films, *i.e.*, there are no extreme peaks on the sample surface. To evaluate further the effect of Mn impurity on the surface morphology of GaN thin films, we analyse the surface skewness (S_{sk}) and coefficient of kurtosis (S_{ka}) parameters, which are sensitive to the presence of isolated deep valleys or high peaks [23]. For both types of films, the value of $S_{sk} > 0$, and for the

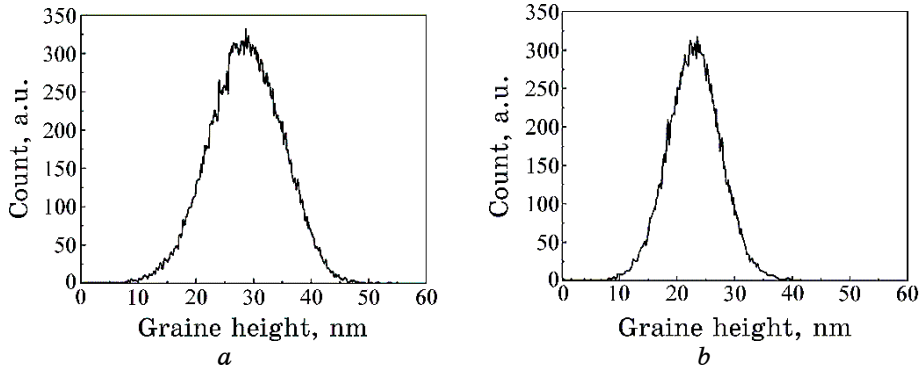

Fig. 2. Grain height distribution on AFM images of as-deposited GaN (*a*) and GaN:Mn (*b*) thin films obtained by RF sputtering on Si substrates.

as-deposited GaN thin film, the value is 0.08, while for the as-deposited GaN:Mn film, this value is 2.5 times higher and amounts to 0.20. The surface morphology of both undoped and Mn-doped GaN thin films are characterized by a large number of protruding peaks above the valleys. For pure as-deposited GaN thin films, an almost symmetrical grain height distribution is observed, which is consistent with the S_q/S_a ratio data and the analysis of height histograms, while in the as-deposited Mn-doped GaN films, the surface is formed with a larger number of protruding peaks (crystallites). The S_{ka} value for as-deposited GaN and GaN:Mn thin films is greater than 3, indicating that the surfaces of both samples contain a significant number of pronounced peaks.

Various factors can influence the formation of the surface morphology of thin films, such as the methods of production and the thermal treatment process of thin films, in which both the annealing temperature and the annealing atmosphere in which the thermal treatment process takes place play significant roles. The type of substrate and the presence of buffer sublayers have different effects on the formation of the surface morphology of the samples. In work [24] investigated the influence of $MgAl_2O_4$, AlN, and ZnO buffer layers on the crystallite size in GaN thin films and found that the smallest crystallite sizes and highest mechanical stresses are characteristic of GaN thin films deposited on quartz substrates with a $MgAl_2O_4$ buffer layer. In Ref. [25], the evolution of the surface morphology of GaN films grown by molecular beam epitaxy on Si(111) substrates using AFM was studied as a function of layer thickness, and two different models of morphology formation behaviour depending on the GaN layer thickness were identified. In Ref. [26], the structural, morphological, and magnetic properties of GaN:Tb and AlGaN:Tb films obtained by ion implantation of Tb^+ into *c*-oriented (0001) GaN and AlGaN films followed by thermal annealing were investigated. The effect of impurities and annealing on changes in surface morphology was studied using AFM, and it was shown that the annealing process effectively repairs crystal defects and reduces surface roughness caused by the ion activator.

To better understand the formation of the surface morphology of as-deposited GaN and GaN:Mn thin films obtained by RF ion-plasma sputtering on Si substrates, we analyse the grain size distributions that form the surface of the studied samples. The characteristic grain diameter size distributions of GaN and GaN:Mn thin films are shown in Fig. 3.

In a comprehensive review [27], it is noted that polycrystalline thin films with thicknesses up to 1 μm often exhibit 2*D*-like structures in which most grain boundaries are perpendicular to the film surface. Perpendicular grain growth to the surface is also charac-

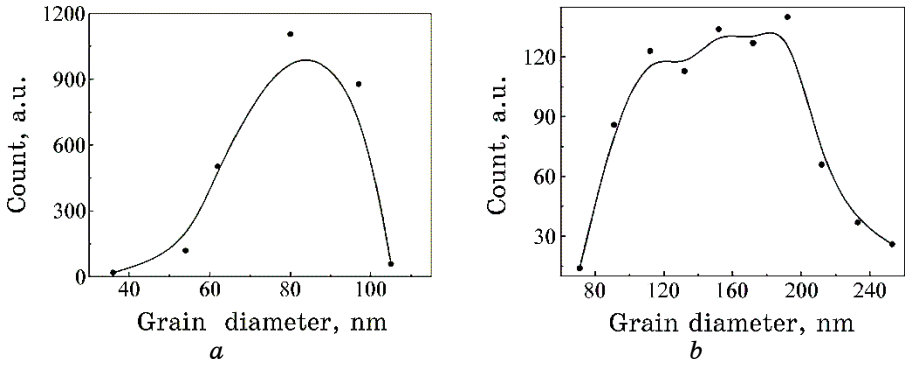

Fig. 3. Grain diameter size distribution and the calculated fitted diameter distribution from AFM images of as-deposited GaN (*a*) and GaN:Mn (*b*) thin films obtained by RF sputtering on Si substrates.

teristic of our GaN films. For most materials analysed in Ref. [27], films are formed from non-equilibrium grains with sizes smaller than the film thickness and form two-dimensional structures only after annealing. In general, the grain sizes in polycrystalline films are lognormally distributed. In a number of cases, further grain growth occurs due to 'abnormal' growth or the preferential growth of several grains, which usually have specific crystallographic orientation relationships with respect to the substrate surface plane. Our results indicate that such a situation is most likely characteristic of the GaN:Mn films we obtained. When the number of growing grains leads to the formation of a grain 'matrix' beyond static boundaries, a bimodal grain size distribution develops and is referred to as secondary grain growth [28]. Grains that grow abnormally often exhibit a limited or uniform texture. The growth of secondary grains in thin films typically involves evolution in the distribution of grain textures as well as evolution in the distribution of grains by size.

Our results for the grain diameter size distribution in GaN and GaN:Mn thin films obtained by RF ion-plasma sputtering (Fig. 3) indicate that for GaN films deposited on Si substrates, a unimodal diameter distribution with a peak at approximately 80 nm is observed (Fig. 3, *a*). A more complex diameter distribution is formed when GaN:Mn thin films are deposited (Fig. 3, *b*). For these films, three local maxima appear in the diameter distribution at approximately 112, 152, and 192 nm, indicating the appearance of a trimodal diameter distribution. The diameter distributions (Fig. 3) and the average diameter sizes values (Table) indicate that during the deposition process of GaN films, the addition of Mn impurity leads to a change in surface energy and promotes the 'coalescence' of

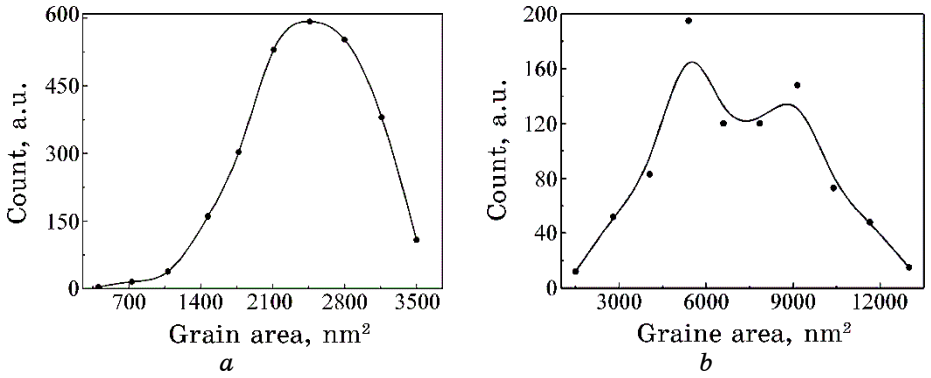

Fig. 4. Grain area size distribution and the calculated fitted area distribution from AFM images of GaN (*a*) and GaN:Mn (*b*) thin films obtained by RF sputtering on Si substrates.

grains into larger formations during film growth. In these films, secondary and tertiary grain growth was observed during the RF sputtering process.

The grain area distribution for sputtered GaN thin films deposited on Si substrates is also characterized by a normal distribution, whereas for as-deposited GaN:Mn thin films on Si substrates, the distribution has a more complex shape, exhibiting two maxima that indicate a bimodal grain area distribution (Fig. 4).

For a more detailed analysis, let us consider the grain volume distribution in GaN and GaN:Mn thin films obtained by RF ion-plasma sputtering on Si substrates. The characteristic grain volume size distributions of GaN and GaN:Mn thin films are shown in Fig. 5.

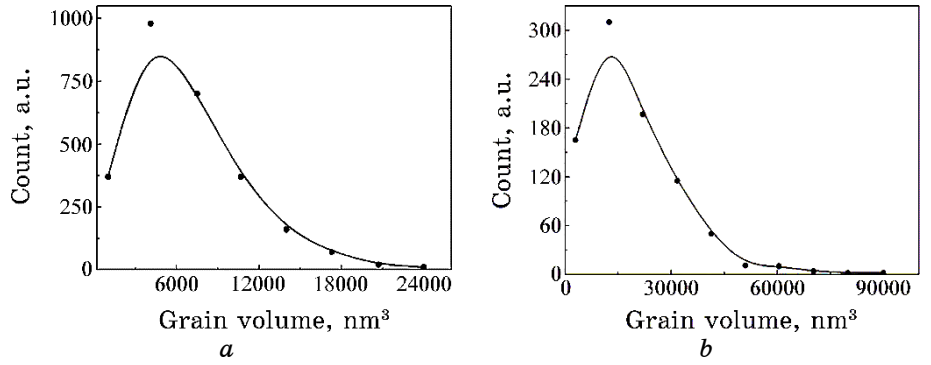

Fig. 5. Grain volume size distribution and the calculated fitted volume distribution from AFM images of GaN (*a*) and GaN:Mn (*b*) thin films obtained by RF sputtering on Si substrates.

As shown in Fig. 5, the grain volume distribution for the GaN and GaN:Mn thin films deposited on Si substrates is fairly well described by a lognormal law. Such behaviour is typical for grain diameter distributions in polycrystalline films [29]. The results of the grain volume distributions are in good agreement with the previously discussed ratio of the root-mean-square surface roughness to the average arithmetic roughness, as well as with the grain height histograms forming the surface of the studied samples, and are described by a normal statistical distribution.

For GaN:Mn thin films obtained by RF sputtering on Si substrates, the grain size distributions, specifically, by diameter and area, exhibit a more complex behaviour. This can be explained by the formation of non-equilibrium grains on the Si substrate upon the addition of Mn dopant, which changes the film growth mechanism compared to undoped films.

To understand better the AFM surface morphology results of GaN and GaN:Mn thin films, Fig. 6 presents an AFM image of the Si substrate surface onto which the studied samples were deposited.

The AFM image in Fig. 6 shows the surface of the Si substrate, which is characterized by linear traces of mechanical polishing and isolated local protrusions, without signs of morphology formation typical for the surface of films deposited on this substrate.

The surface morphology results of GaN and GaN:Mn thin films obtained by AFM are in good agreement with the results recorded using SEM. Figure 7 shows SEM images of the surface morphology of GaN, GaN:Mn, and GaN:Tb thin films.

The SEM results (Fig. 7) correlate well with the AFM data for GaN and GaN:Mn thin films. The as-deposited undoped GaN thin film is characterized by a fine-grained structure (Fig. 7, *a*), which is confirmed by the smaller average grain sizes determined from the AFM images (Fig. 1 and Table). The SEM images of the surface of GaN:Mn and GaN:Tb samples indicate a significant influence of the impurity and its type on the formation of the film surface morphology. The introduction of Mn impurity leads to an increase in grain size, as evidenced by the increase in their average diameter, area, and volume from AFM data, accompanied by a decrease in surface roughness parameters S_a and S_q (Fig. 1 and Table). In the GaN crystal lattice, Mn atoms relatively easily replace Ga atoms, since the ionic radius of Mn^{2+} (0.66 Å) is close to the ionic radius of Ga^{3+} (0.62 Å) [30]. The grain boundaries in GaN:Mn thin films become more distinct, and the grain peaks appear flatter. In the case of Tb doping, the films exhibit an even larger grain structure, indicating a change in the nucleation and crystallite growth mechanisms. It is likely that the large ionic radius of terbium Tb^{3+} (0.92 Å) [31] creates such strong stresses that the film begins to grow more uneven-

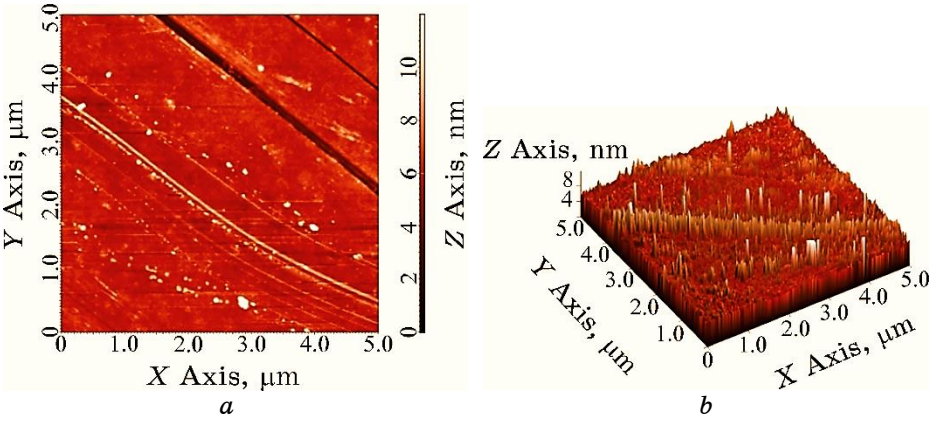

Fig. 6. 2*D* (*a*) and 3*D* (*b*) AFM images of the surface morphology of the Si substrate.

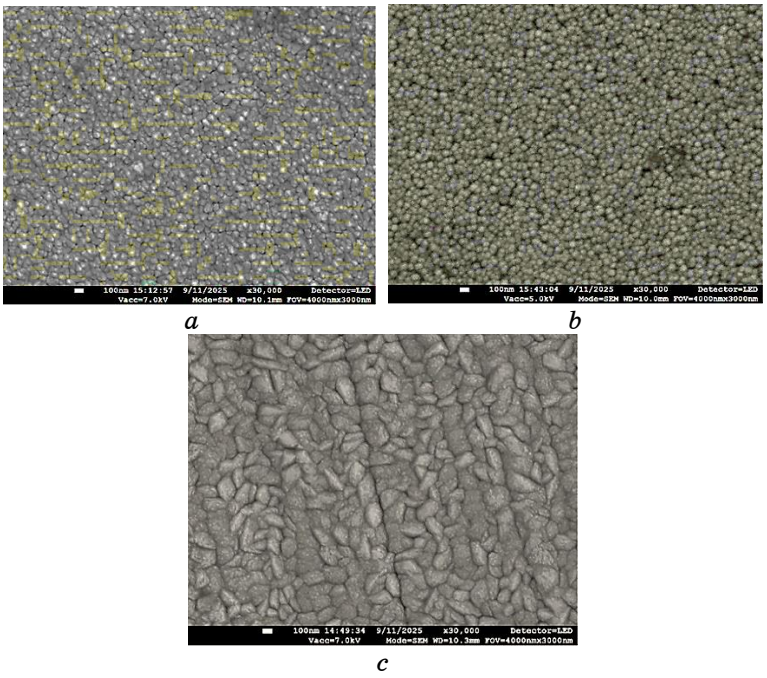

Fig. 7. SEM images of the surface morphology of as-deposited GaN (*a*), GaN:Mn (*b*), and GaN:Tb (*c*) thin films obtained by RF sputtering on Si substrates.

ly with large grain sizes.

The obtained results indicate that transition and rare-earth ele-

ment impurities significantly influence the formation of the surface structure of GaN films.

4. CONCLUSIONS

It has been established that RF ion-plasma sputtering onto single-crystal Si substrates results in the formation of GaN and GaN:Mn thin films composed of nanometer-sized grains. Based on AFM images, it was shown that the average grain diameter is 85 nm for GaN thin films and increases to 166 nm for GaN:Mn films. It was found that for GaN:Mn thin films, the root-mean-square and average-arithmetic surface roughness values are 4.8 and 3.8, respectively, which are 1.3 times lower than the corresponding values for the as-deposited GaN film. Based on the analysis of the grain diameter size distributions, it is shown that GaN films exhibit a unimodal distribution, whereas GaN:Mn films follow a trimodal distribution. Based on the analysis of the grain diameter size distributions, it is proposed that secondary and tertiary grain growth processes occur during the RF sputtering process. Based on the analysis of the grain volume distribution results, it is shown that, in both cases, the grain volume distribution follows a lognormal law. Comparison of AFM and SEM results showed that the surface morphology depends on the type of impurity, and the introduction of Tb^{3+} with a larger ionic radius (0.92 Å) leads to significant structural stresses and the formation of a pronounced coarse-grained structure.

REFERENCES

1. Chunyu Zhao, Swee Tiam Tan, and Hilmi Volkan Demir, *Semicond. Sci. Technol.*, **40**: 073001 (2025); https://doi.org/10.1088/1361-6641/ade81f
2. K. Murakawa, Y. Kawaguchi, M. Usagawa, Y. Tanabe, T. Yokoyama, M. Tonomura, Y. Aoki, K. Takeuchi, and T. Kamikawa, *Optics Express*, **33**, No. 3: 4100 (2025); https://doi.org/10.1364/OE.542386
3. Toshihiko Fukamachi, Junichi Nishinaka, Koichi Naniwae, Shuichi Usuda, Haruki Fukai, Akihiko Sugitani, Masahiro Uemukai, Tomoyuki Tanikawa, and Ryuji Katayama, *Japanese Journal of Applied Physics*, **64**: 022001 (2025); https://doi.org/10.35848/1347-4065/ada903
4. A. Dubey, R. Mishra, Yu-H. Hsieh, Ch.-W. Cheng, B.-H. Wu, L.-J. Chen, S. Gwo, and T.-J. Yen, *Adv. Sci.*, **7**: 2002274 (2020); doi:10.1002/advs.202002274
5. E. Yilmaz, H. Wang, E. Doganci, M. Feng, Q. Sun, A. Mutale, A. Kahraman, U. Gurer, O. Yilmaz, A. Sadigov, F. Ahmadov, and E. Budak, *IEEE Transactions on Electron Devices*, **72**, No. 4: 1993 (2025); doi:10.1109/TED.2025.3539636
6. J. Zhang, L. Deng, S. Xia, C. Guo, K. Liu, L. Chen, W. Liu, H. Xiao, Zh. Yang, W. Guo, and J. Ye, *Semicond. Sci. Technol.*, **39**: 073001 (2024);

https://doi.org/10.1088/1361-6641/ad5100
7. Zitong Fan, *IOP Conf. Series: Materials Science and Engineering*, **738**: 012006 (2020); doi:10.1088/1757-899X/738/1/012006
8. H. J. Lozykowski, W. M. Jadwisienczak, and I. Brown, *Materials Science and Engineering: B*, **81**, Iss. 1–3: 140 (2001); https://doi.org/10.1016/S0921-5107(00)00697-8
9. J. Laski, J. H. Tao, K. Mishra, D. Hamby, M. Raukas, K. Klinedinst, J. McKittrick, J. B. Talbot, N. Perea-Lopez, and G. Hirata, *ECS Transactions*, **16**, No. 31: 123 (2009); https://doi.org/10.1149/1.3112647
10. M. Stachowicz, A. Kozanecki, C.-G. Ma, M. G. Brik, J. Y. Lin, Hx. Jiang, and J. M. Zavada, *Optical Materials*, **37**: 165 (2014); http://dx.doi.org/10.1016/j.optmat.2014.05.018
11. Or H. Chaulker, Yury Turkulets, and Ilan Shalish, *Scientific Reports*, **15**: 18773 (2025); https://doi.org/10.1038/s41598-025-97446-w
12. Wenxuan Wu, Yangye Pan, Xiaodong Gao, Xiaodan Wang, Sida Wei, Jiahao Sun, Xionghui Zeng, Shunan Zheng, and Ke Xu, *J. Phys. D: Appl. Phys.*, **58**: 135101 (2025); https://doi.org/10.1088/1361-6463/ada8bb
13. Michael Alexander Reshchikov, Benjamin McEwen, and Shadi Shahedipour-Sandvik, *phys. status solidi (b)*, **262**: 2400656 (2025); doi:10.1002/pssb.202400656
14. Y. Xiong, M. Sadek, and R. Chu, *Semicond. Sci. Technol.*, **40**: 033002 (2025); https://doi.org/10.1088/1361-6641/adb32d
15. H. Amano, Y. Baines, E. Beam, Matteo Borga, T. Bouchet, Paul R. Chalker, M. Charles, Kevin J. Chen, Nadim Chowdhury, Rongming Chu, Carlo De Santi, Maria Merlyne De Souza, Stefaan Decoutere, L. Di Cioccio, Bernd Eckardt, Takashi Egawa, P. Fay, Joseph J. Freedsman, L. Guido, Oliver Häberlen, Geoff Haynes, Thomas Heckel, Dilini Hemakumara, Peter Houston, Jie Hu, Mengyuan Hua, Qingyun Huang, Alex Huang, Sheng Jiang, H. Kawai, Dan Kinzer, Martin Kuball, Ashwani Kumar, Kean Boon Lee, Xu Li, Denis Marcon, Martin März, R. McCarthy, Gaudenzio Meneghesso, Matteo Meneghini, E. Morvan, A. Nakajima, E. M. S. Narayanan, Stephen Oliver, Tomás Palacios, Daniel Piedra, M. Plissonnier, R. Reddy, Min Sun, Iain Thayne, A. Torres, Nicola Trivellin, V. Unni, Michael J. Uren, Marleen Van Hove, David J. Wallis, J. Wang, J. Xie, S. Yagi, Shu Yang, C. Youtsey, Ruiyang Yu, Enrico Zanoni, Stefan Zeltner, and Yuhao Zhang, *J. Phys. D: Appl. Phys.*, **51**: 163001 (2018); https://doi.org/10.1088/1361-6463/aaaf9d
16. C. Braun, L. Mereacre, Z. Chen, and A. Slabon, *Scientific Reports*, **12**: 2503 (2022); https://doi.org/10.1038/s41598-022-06148-0
17. Heesoo Kim, Anh Thi Dieu Nguyen, Beomjun Kim, Hyerin Jo, Imasda Rahmatulloh, Hyobin Yoo, Hongseok Oh, Aziz Ahmed, Hyeonjun Beak, and Kunook Chung, *NPG Asia Materials*, **17**: 13 (2025); https://doi.org/10.1038/s41427-025-00594-8
18. Mandar A. Kulkarni, Hyesu Ryu, Sohyeon Park, Tae Kyoung Kim, Sangjin Min, Seung Hyun Shin, Hamza Thaalbi, Fawad Tariq, Sang Hyun Lee, Ho Won Jang, Joon Seop Kwak, Dong-Soo Shin, Pyoung Gug Kim, Sang-Wan Ryu, *Adv. Optical Mater.*, **13**: 2500271 (2025); doi:10.1002/adom.202500271
19. Xiaoqin Yang, Jiawen Lu, Luyu Zhao, Xiaorui Han, Zhongwei Bai, Peiwen Quan, Liangshuai Xie, Liang Li, Haoxuan Sun, Mark Hermann Rummeli,

Bingcheng Luo, and Hong Gu, *Adv. Photonics Res.*, **6**: 2400146 (2025); doi:10.1002/adpr.202400146
20. K. Wasa, M. Kitabatake, and H. Adachi, *Thin Film Materials Technology: Sputtering of Compound Materials* (New York: Springer–William Andrew Inc Publishing: 2004).
21. O. M. Bordun, I. Yo. Kukharskyy, M. V. Protsak, I. I. Medvid, I. M. Kofliuk, Zh. Ya. Tsapovska, and D. S. Leonov, *Nanosistemi, Nanomateriali, Nanotehnologii*, **22**, Iss. 2: 287 (2024); https://doi.org/10.15407/nnn.22.02.287
22. B. Rajesh Kumar and T. Subba Rao, *Digest Journal of Nanomaterials and Biostructures*, **7**, No. 4: 1881 (2012); https://storage.imrpress.com/IMR/DJNB/7/4/1881_RajeshKumar.pdf
23. E. S. Gadelmawla, M. M. Koura, T. M. A. Maksoud, I. M. Elewa, and H. H. Soliman, *Journal of Materials Processing Technology*, **123**, Iss. 1: 133 (2002); https://doi.org/10.1016/S0924-0136(02)00060-2
24. O. M. Bordun, I. Yo. Kukharskyy, M. V. Protsak, I. I. Medvid, I. O. Bordun, I. M. Kofliuk, I. S. Kuz, A. I. Tyslyuk, R. V. Pavlius, and D. S. Leonov, *Nanosistemi, Nanomateriali, Nanotehnologii*, **23**, Iss. 3: 771 (2025); https://doi.org/10.15407/nnn.23.03.0771
25. S. Vézian, F. Natali, F. Semond, and J. Massies, *Physical Review B*, **69**: 125329 (2004); doi:10.1103/PhysRevB.69.125329
26. X. Gao, C. Liu, C. Yin, D. Tao, C. Yang, and B. Man, *Materials Science and Engineering B*, **178**: 349(2013); http://dx.doi.org/10.1016/j.mseb.2012.12.005
27. C. V. Thompson, *Sol. State Phys.*, **55**: 269 (2001); https://doi.org/10.1016/S0081-1947(01)80006-0
28. C. V. Thompson, *J. Appl. Phys.*, **58**: 763 (1985); https://doi.org/10.1063/1.336194
29. J. E. Palmer, C. V. Thompson, and Henry I. Smith, *J. Appl. Phys.*, **62**, No. 6: 2492 (1987); http://dx.doi.org/10.1063/1.339460
30. Yoon Shon Hae Kwon, Deuk Young Kim, and Xiangjun Fan Won Kang, *Jpn. J. Appl. Phys.*, **40**: 5304 (2001); https://doi.org/10.1143/JJAP.40.5304
31. Natalie T. Rice, Ivan A. Popov, Dominic R. Russo, John Bacsa, Enrique R. Batista, Ping Yang, Joshua Telser, and Henry S. La Pierre, *J. Am. Chem. Soc.*, **141**, No. 33: 1 (2019); doi:10.1021/jacs.9b06622